ACS APPLIED MATERIALS & INTERFACES

Research Article

www.acsami.org

Polymer-Coated Hollow Mesoporous Silica Nanoparticles for Triple-Responsive Drug Delivery

Yuanyuan Zhang,[†] Chung Yen Ang,[†] Menghuan Li,[†] Si Yu Tan,[†] Qiuyu Qu,[†] Zhong Luo,[†] and Yanli Zhao*[,†,‡]

[†]Division of Chemistry and Biological Chemistry, School of Physical and Mathematical Sciences, Nanyang Technological University, 21 Nanyang Link, 637371 Singapore

[‡]School of Materials Science and Engineering, Nanyang Technological University, 50 Nanyang Avenue, 639798 Singapore

Supporting Information

ABSTRACT: In this study, pH, reduction and light triple-responsive nanocarriers based on hollow mesoporous silica nanoparticles (HMSNs) modified with poly(2-(diethylamino)-ethyl methacrylate) (PDEAEMA) were developed via surface-initiated atom transfer radical polymerization. Both reduction-cleavable disulfide bond and light-cleavable *o*-nitrobenzyl ester were used as the linkages between HMSNs and pH-sensitive PDEAEMA polymer caps. A series of characterization techniques were applied to characterize and confirm the structures of the intermediates and final nanocarriers. Doxorubicin (DOX) was easily encapsulated into the nanocarriers with a high loading capacity, and quickly released in response to the stimuli of reducing agent, acid environment or UV light irradiation. In addition, flow cytometry analysis, confocal laser scanning microscopy observations and cytotoxicity studies indicated that the nanocarriers were efficiently internalized by HeLa cancer cells, exhibiting (i) enhanced release of DOX into the cytoplasm under external UV light irradiation, (ii) better cytotoxicity against HeLa cells, and (iii) superior control over drug delivery and release. Thus, the triple-responsive nanocarriers present highly promising potentials as a drug delivery platform for cancer therapy.

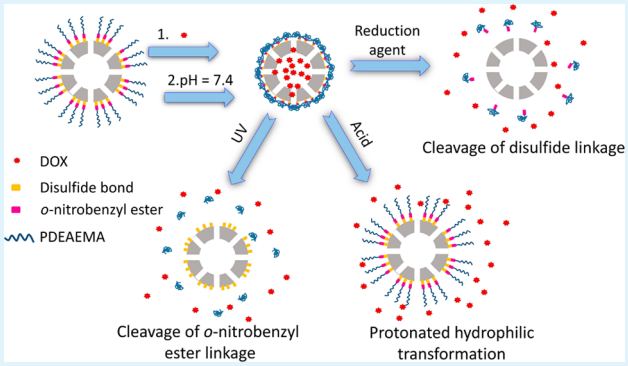

KEYWORDS: *controlled drug delivery, hollow mesoporous silica nanoparticles, nanocarriers, polymer coating, triple-responsive release*

1. INTRODUCTION

Mesoporous silica nanoparticles (MSNs) have been extensively studied as therapeutic drug nanocarriers because of their unique features such as tunable pore size, relative high surface area, excellent stability, favorable biocompatibility, and easy surface functionalization.[1−4] Because of to their nanoscale size, the blood circulation time of MSNs could be significantly prolonged, and at the same time, they could be selectively accumulated at the tumor sites via the enhanced permeability and retention (EPR) effect.[5,6] In regard to the biosafety issues in clinic, it is desirable to use lower amount of drug nanocarriers with higher drug loading capability for the drug delivery application.[7,8] Hollow MSNs (HMSNs) have been developed with increasing attention,[9,10] because HMSNs possess large hollow interiors for the storage of more cargos in comparison with conventional MSNs.

For unmodified MSN-based nanocarriers, their therapeutic efficiency is usually compromised by the prerelease of physically loaded drug molecules during the blood circulation,[11] which accounts for a low level of drug accumulation in the target cancer cells and undesired damage to healthy cells and organs. To improve their therapeutic efficacy and minimize the side effects, various types of stimuli-responsive MSN-based drug nanocarriers have been designed with on-demand and controlled drug release features after being endocytosed by cancer cells.[12,13] Compared with widely reported MSNs functionalized with inorganic nanoparticles,[14,15] organic compounds,[16,17] or biological species,[18,19] MSNs coated with responsive polymers are of special interests due to the diversity, multifunctional capability, and excellent drug-controlling capacity of the polymer structures.[20] Various stimuli-responsive polymers have been utilized to functionalize MSNs so as to control the release of loaded drugs. For example, given lower pH values in the endo/lysosomal compartments of cancer cells,[21] pH-responsive polymers such as poly(2-(diethylamino)-ethyl methacrylate) (PDEAEMA),[22,23] poly(2-phenyl-1,3-dioxan-5-yl methacrylate),[24] and poly(acrylic acid)[25] were proposed to be anchored on MSNs to achieve acid-triggered drug release. Another example is the utilization of disulfide bond, one of biocleavable linkages, to cross-link the grafted polymer shell to control the release of cargos loaded inside MSNs.[26] Compared with these biological stimuli that are innate properties of cancer

Received: July 1, 2015
Accepted: July 29, 2015
Published: July 29, 2015

ACS Publications © 2015 American Chemical Society

DOI: 10.1021/acsami.5b05893
ACS Appl. Mater. Interfaces 2015, 7, 18179−18187

Scheme 1. Schematic Representation for the Structure of HMSNs-PDEAEMA and Different Mechanisms of Triggered Drug Release

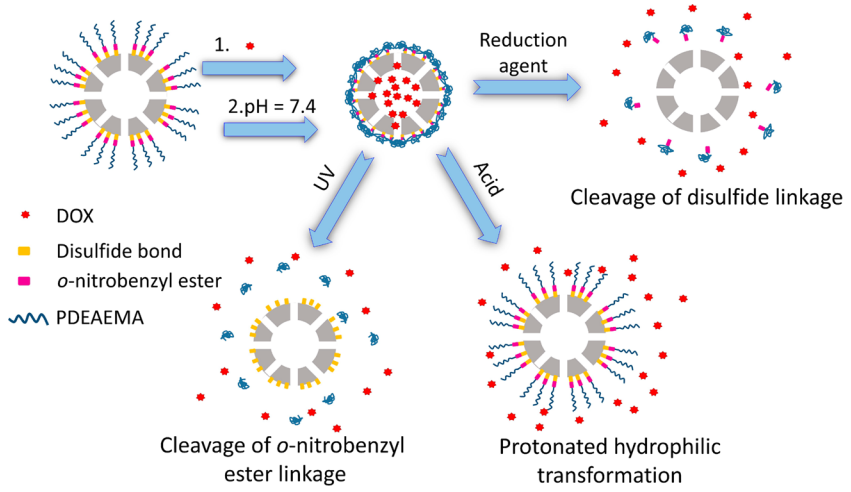

cells, external triggers such as light illumination are even more advantageous for their superior controllability, because they could provide remote control of the doses and timing to drug-loaded nanocarriers. Thus, polymers containing photoresponsive groups such as coumarin,[27] *o*-nitrobenzyl ester (ONB),[28] spiropyran,[29] and azobenzene[30] were utilized to coat MSNs for achieving light-triggered drug release. These designs greatly expand the application scope of functional polymer coating in drug delivery systems, allowing for the development of more versatile stimuli-responsive MSN-based nanocarriers.

In an effort to further improve chemotherapeutic performance, two or more stimuli-responsive mechanisms could be practically combined into one drug delivery system to meet various requirements under complicated physiological environment.[31,32] Notably, these multistimuli-responsive drug delivery systems possess all the advantages of individual stimulus approaches at the same time, showing unprecedented control over drug delivery to pathological sites for subsequent drug release.[33,34] The multiresponse design is not only capable of responding to individual stimulus for controlled drug release, but also exhibits enhanced release when triggered with multiple stimuli simultaneously. For example, Zhang et al.[35] reported functional MSNs coated with pH and redox dual-responsive polymer consisting of acid-hydrolyzable benzoic-imine bond and reduction-cleavable disulfide linkage. Another example with similar stimuli-responsive property was developed by Wang et al.[36] using disulfide bond cross-linked poly[(*N*-vinylcaprolactam)-*co*-(methacrylic acid)] as the gate keeper of MSNs to control the drug release. Liu and co-workers[36] investigated the release behavior of pH and thermo dual-responsive MSNs coated by sensitive poly[(*N*-isopropylacrylamide)-*co*-(methacrylic acid)]. Nevertheless, MSN-based nanocarriers with more than two stimuli-responsive pathways have not been reported so far to the best of our knowledge. Considering sophisticated blood circulation environment for drug delivery, the integration of multistimuli responses into single nanocarrier for more precise control of drug release is necessary and important.

Scheme 1 shows a facile strategy of preparing triple-responsive HMSNs as nanocarriers in this study. Initiating group functionalized HMSNs were coated with PDEAEMA via surface-initiated atom transfer radical polymerization (ATRP) to retain the encapsulated drug inside. In neutral or alkaline (e.g., pH 7.4) environments, PDEAEMA polymer chains would be in a collapsed state,[37,38] thus effectively inhibiting the drug diffusion out of the HMSN channels. On the contrary, in acidic conditions (e.g., pH 5), the protonated polymer chains would adopt extended conformation, allowing the opening of mesopores for the drug release. In addition, the pH-sensitive PDEAEMA was anchored on the surface of HMSNs via both reduction-cleavable disulfide bond and photolabile ONB linkage. The disulfide bond is stable under physiological conditions, but could be readily cleaved under reducing environment.[39,40] The photolabile ONB group could undergo rapid isomerization when exposed to UV light at 365 nm, leading to the cleavage of the chromophore for subsequent drug release.[41,42]

This design has several distinctive advantages: (1) higher DOX loading capacity owing to the hollow interiors of HMSNs; (2) excellent stability during the blood circulation as compared to pure polymeric micelle/vesicle-based drug delivery systems;[43,44] (3) efficient response to triple stimuli of reducing agents, acid environment, as well as external UV irradiation, and (4) on account of reversible opening and closure of the mesopores by pH-responsive PDEAEMA, the drugs can be simply loaded and capped in the mesopores under mild conditions by adjusting pH values of the sample suspension.

2. EXPERIMENTAL SECTION

2.1. Materials and Reagents. Toluene (Sigma-Aldrich) was dried with CaH_2 and redistilled under reduced pressure before use. All other solvents were bought from Merck and used without purification. 2-(Diethylamino)ethyl methacrylate (DMAEMA, Sigma-Aldrich) was passed through a activated basic alumina column to remove the inhibitors before use. Copper(I) bromide (CuBr, Sigma-Aldrich) was purified by stirring in acetic acid, washed extensively with ethanol, and finally dried under vacuum. Azidoacetic acid, copper(II) sulfate pentahydrate ($CuSO_4{\cdot}5H_2O$), dithiothreitol (DTT), doxorubicin hydrochloride (DOX·HCl), ethylenediaminetetraacetic acid (EDTA), 3-mercaptopropyl-trimethoxysilane (MPTS), *N*,*N*,*N*′,*N*″,*N*″-pentamethyldiethylenetriamine (PMDETA), and sodium ascorbate were all purchased from Sigma-Aldrich and used without purification. Acetic acid, *N*-hydroxysuccinimide (NHS), and *N*-(3-(dimethylamino)-propyl)-*N*′-ethylcarbodiimide (EDC) were obtained from Alfa and used as received. *S*-(2-Aminoethylthio)-2-thiopyridine hydrochloride and 5-propargylether-2-nitrobenzyl bromoisobutyrate were prepared according to procedures reported in literature.[45,46]

DOI: 10.1021/acsami.5b05893
ACS Appl. Mater. Interfaces 2015, 7, 18179−18187

2.2. Instruments. ^{1}H nuclear magnetic resonance (NMR) spectra were recorded on a Bruker BBFO-400 using deuterated chloroform ($CDCl_3$) as the solvent. Scanning electron microscopy (SEM) images were obtained on JSM-7100F (JEOL) at 100 kV. Transmission electron microscopy (TEM) images were collected on JEM-1400 (JEOL) at 100 kV. The fluorescence intensities were measured by fluorescence spectrophotometer (RF5301PC, Shimadzu, Japan). The UV−vis absorption intensities were recorded on UV-3600 spectrophotometer (Shimadzu). Zeta-potential values were determined by a Malvern Instruments Zetasizer Nano-S at 25 °C. X-ray photoelectric spectroscopy (XPS) was obtained on a Phoibos 100 spectrometer with a SPECS monochromatic Mg X-ray radiation source (wide-range and high resolution S 2p scans at 12.53 kV). The specific surface areas were determined from the adsorption data in low pressure range following the Brunauer−Emmett−Teller (BET) model, and pore size was calculated using the Barret-Joyner-Halenda (BJH) method. Thermogravimetric analysis (TGA) was performed using a TGA-Q500 recorded from 100 to 1000 °C in an air flow at a heating rate of 10 °C min^{-1}.

2.3. Synthesis of *o*-Nitrobenzyl Linkage. 5-Propargylether-2-nitrobenzyl bromoisobutyrate (0.710 g, 2.00 mmol) and azidoacetic acid (0.224 g, 2.20 mmol) were dissolved in the mixture of THF/water (v/v = 8:1, 30 mL), followed by the addition of sodium ascorbate (0.079 g, 0.20 mmol) and $CuSO_4{\cdot}5H_2O$ (0.050 g, 0.20 mmol). The solution was allowed to stir at room temperature for 6 h. After the removal of the solvent under reduced pressure, the crude product was purified by silica gel column chromatography (CH_2Cl_2/MeOH, v/v = 20:1) to obtain the product HOOC-NBO-*i*BuBr as a brown solid. Yield: 94%. ^{1}H NMR ($CDCl_3$, 400 MHz,): δ 1.94 (s, 6H, CH_3), 5.30 (s, 6H, triazole-CH_2-Ar), 5.36 (s, 2H, HOOC-CH_2-), 5.58 (s, 2H, -CH_2-OCO-), 7.29 (d, 1H, J = 8.4 Hz, Ar-*H*), 7.32 (s, 1H, Ar-*H*), 8.19 (d, 1H, J = 8.4 Hz, Ar-*H*), 8.27 (s, 1H, triazole-*H*). ^{13}C NMR (400 MHz, $CDCl_3$): δ 30.2, 50.6, 57.0, 61.8, 64.2, 114.4, 114.8, 126.4, 128.0, 134.2, 140.1, 141.6, 162.2, 168.5, 170.3. TOF HRMS: calcd. for $C_{16}H_{17}BrN_4O_7$ $[M + H]^+$, 457.2370; found, 457.0359. The relevant characterization spectra are presented in Figures S1−S3.

2.4. Synthesis of Disulfide-Modified HMSNs. First, the HMSNs with cetyltrimethylammonium bromide (CTAB) as the surfactant template (HMSNs@CTAB) were prepared according to the literature report and Na_2CO_3 was used as the etching reagent to selectively remove the solid silica core.[47,48] The obtained HMSNs@CTAB (0.8 g) were suspended in anhydrous toluene (80 mL) containing MPTS (0.6 mL), and the mixture was stirred gently at 60 °C for 36 h. After centrifugation, the nanoparticles were extensively washed with absolute ethanol to remove excess MPTS. To extract the CTAB template, the above prepared nanoparticles (0.6 g) were resuspended in MeOH (150 mL), to which a concentrated hydrochloric acid solution (37%, 10 mL) was added, and the suspension was refluxed at 80 °C for 48 h. Finally, CTAB-removed nanoparticles HMSNs-SH were obtained by centrifugation, washed thoroughly with ethanol, and eventually dried under vacuum.

Second, disulfide bond with terminal amino group was immobilized. Basically, HMSNs-SH (0.5 g) was dispersed in the mixture of ethanol (30 mL) and acetic acid (1.2 mL). Then, the suspension was added with *S*-(2-aminoethylthio)-2-thiopyridine hydrochloride (0.5 g) and stirred at room temperature for 48 h. The resultant disulfide-bond-containing nanocarriers, denoted as HMSNs-NH_2, were washed exclusively with ethanol and finally dried under vacuum.

2.5. Functionalization with ATRP Initiating Group. HMSNs-NH_2 was modified with HOOC-NBO-*i*BuBr via an amidation reaction in the presence of EDC and NHS. To a stirring solution of HOOC-NBO-*i*BuBr (91.4 mg, 0.20 mmol) in anhydrous DMF (5 mL) was added with EDC (46.0 mg, 0.24 mmol) and NHS (27.6 mg, 0.24 mmol) at 0 °C. The resulting turbid solution was stirred at room temperature for 3 h before the DMF suspension (30 mL) of HMSNs-NH_2 (0.3 g) was added. After stirring at room temperature for 10 h, the ATRP initiating group modified nanoparticles, denoted as HMSNs-Br, were washed two times with DMF, four times with ethanol and then dried under vacuum.

2.6. Synthesis of PDEAEMA-Coated HMSNs via ATRP. Briefly, HMSNs-Br (0.10 g), DEAEMA (1.38 g, 7.50 mmol) and PMDETA (87.0 mg, 0.50 mmol) were dispersed in methanol (5 mL) in a reaction tube. After degassing by freeze−pump−thaw for three cycles, CuBr (36 mg, 0.25 mmol) was introduced into the mixture under N_2 protection and the reaction mixture was stirred at 70 °C for 24 h. After exposing to air to stop the polymerization, PDEAEMA coated nanoparticles, denoted as HMSNs-PDEAEMA, were centrifuged. Then, the nanoparticles were washed three times with DMF to extract the ungrafted polymer or free reagents and two times with 5% EDTA solution to remove any copper residue. After additional washing three times with ethanol, the nanocarriers were dried under vacuum.

To retrieve the grafted polymer for analysis, we suspended HMSNs-PDEAEMA (20 mg) in THF (5 mL), followed by addition of HF (40 w% aqueous solution, 1 mL). The resultant solution was stirred at room temperature overnight. Then, the solution was placed into a dialysis bag (molecular weight cutoff = 3500) and dialyzed against deionized water for 48 h. After lyophilization, the retrieved polymer was subjected to ^{1}H NMR analysis.

2.7. Preparation of DOX-Loaded HMSNs-PDEAEMA. The loading of anticancer drug DOX into HMSNs-PDEAEMA was achieved through the procedures specified below. Typically, HMSNs-PDEAEMA (5.0 mg) and DOX·HCl (2.0 mg) were added into deionized water (1 mL), and the obtained suspension was stirred at room temperature in the dark for 24 h. Then, resultant nanoparticles, denoted as HMSNs@DOX, were obtained by centrifugation and washed extensively with phosphate buffer solution (PBS, pH 7.4, 10 mM) to remove the adsorbed drug until the supernatant solution became colorless. The amount of loaded DOX was determined through the UV−vis absorption at 485 nm by subtracting the amount of unloaded DOX in the collected supernatant from the amount of original feeding DOX. The drug loading content (DLC) and drug loading efficiency (DLE) were calculated according to the equations as shown below

$$\text{DLC (wt \%)} = (\text{weight of loaded drug/weight of HMSNs@DOX})100\%$$

$$\text{DLE (wt \%)} = (\text{weight of loaded drug/weight of feeding drug})100\%$$

2.8. In vitro Drug Release. The release of DOX from HMSNs@DOX triggered by biological stimuli was studied at 37 °C under different conditions: (i) PBS (100 mM, pH 7.4), (ii) acetate buffer solution (100 mM, pH 5.0), (iii) PBS (100 mM, pH 7.4) containing 10 mM DTT, and (iv) acetate buffer solution (100 mM, pH 5.0) containing 10 mM DTT. HMSNs@DOX suspension was first placed into a dialysis bag (molecular weight cutoff = 12 000) and dialyzed against corresponding buffer medium (40 mL) at 37 °C in the dark. At predetermined time intervals, 4.0 mL of the release medium was taken out and analyzed by fluorescence measurements, while the same amount of new buffer solution was added back to the original release medium. The concentrations of the released DOX in the dialysate were calculated according to the intensity of fluorescence emission at 560 nm under the excitation wavelength of 480 nm. In addition, external light triggered release of DOX was also studied in PBS (pH 7.4) without the presence of DTT. At designated times, the sample was subjected to UV light irradiation (365 nm, 20 mW/cm^2) for 10 min, and the fluorescence of the dialysate was measured as described above. After repeating the release experiments for three times independently, the mean value was used as the final result.

2.9. Cellular Uptake by HeLa Cells. Flow cytometry was applied to quantitively evaluate the cellular uptake of the drug delivery system. In this study, HeLa cells, as one of typical cancer cell lines, were cultured with Dulbecco's modified eagle medium (DMEM) containing 10% fetal bovine serum (FBS), penicillin (100 U mL^{-1}) and streptomycin (100 μg mL^{-1}) at 37 °C under 5% CO_2 atmosphere. HeLa cells (2.0×10^5 cells per well) were seeded in a 6-well tissue culture plate with DMEM (2.0 mL) containing 10% FBS. After culturing for 24 h, free DOX or HMSNs@DOX was added in the culture medium, which was equivalent to the DOX concentration at 3 μg mL^{-1} for every well. After the incubation for 3 h, the culture medium was replaced. The cell samples were exposed to UV irradiation (365 nm, 20 mW) for 10 min and incubated for another

DOI: 10.1021/acsami.5b05893
ACS Appl. Mater. Interfaces 2015, 7, 18179−18187

Scheme 2. Synthetic Route of Triple-Responsive HMSNs-PDEAEMA via Surface-Initiated Atom Transfer Radical Polymerization

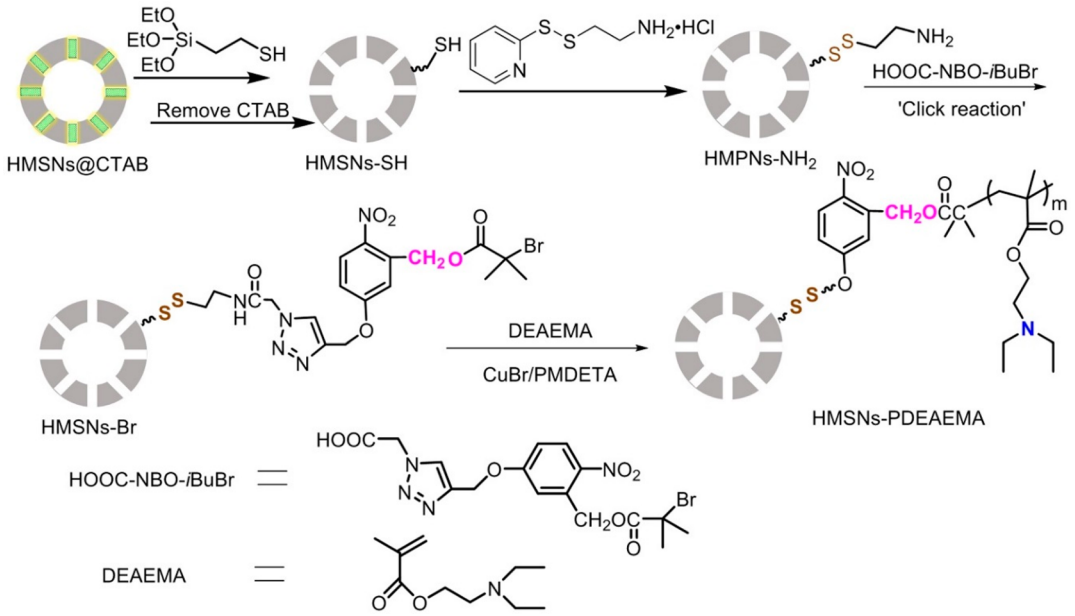

3 h. In addition, cells without UV irradiation were also incubated for comparison. After that, HeLa cells were washed with PBS for several times and treated with trypsin for 2 min. Then, PBS (2.0 mL) was added to each culture well, and the cells were collected via centrifugation at 2000 rpm for 2 min. Finally, the cells were resuspended in PBS (0.4 mL) for the flow cytometry analysis.

Confocal laser scanning microscopy (CLSM) was further employed to observe the intracellular release behavior of HMSNs@DOX within HeLa cells. Briefly, HeLa cells were seeded onto glass coverslips in six-well plates with a cell density at 2×10^5 per well in DMEM (2.0 mL) containing 10% FBS. After culturing for 24 h, the medium was replaced. Then, free DOX (5 μg mL^{-1}) as well as HMSNs@DOX suspension with an equivalent DOX concentration were added into the cell culture media, respectively. After 3 h of incubation, the cell medium was replaced. The cells treated with HMSNs@DOX were irradiated with UV light (365 nm, 20 mW) for 10 min and incubated for another 3 h. In addition, unirradiated cells were incubated for comparison. After washing with PBS, the HeLa cells on the slide were fixed with 4% formaldehyde at room temperature for 15 min. Finally, the samples were stained with 4′6-diamidino-2-phenylindole (DAPI, blue color) for 5 min and mounted for observation with CLSM.

2.10. In Vitro Cytotoxicity Study. The in vitro cytotoxicity of free DOX, HMSNs-PDEAEMA and HMSNs@DOX was quantitatively investigated by using 3-(4,5-dimethylthiazol-2-yl)-2,5-diphenyltetrazolium bromide (MTT) assay. Briefly, HeLa cells in culture medium (100 μL) were seeded in 96-well plates with a density at 1×10^4 cells per well. When the cell confluence reached around 60−70%, the medium was replaced with fresh one (90 μL), and then free DOX solutions or nanoparticle suspensions (10 μL each) with various concentrations were added. After 4 h of incubation, the cultural medium was replaced and the cells were irradiated with UV light (365 nm, 20 mW) for 10 min. The cell groups without any treatment were used as a control. After incubation for 24 h, the medium was replaced again, followed by the addition of MTT solution (10 μL, 5 mg L^{-1}). The cells were incubated for another 4 h, and then the medium was replaced by DMSO (100 μL) to dissolve the resultant purple crystals. Finally, optical intensities of the samples were measured by using a microplate reader (infinite M200, TECAN) at 490 nm. The percentage of cell viability was calculated on the basis of the following equation: $(A_1/A_2)100\%$, where A_1 and A_2 represent the absorbance of the sample and control groups, respectively.

3. RESULTS AND DISCUSSION

3.1. Preparation of HMSNs-PDEAEMA. The triple-responsive HMSNs-PDEAEMA was prepared as described in Scheme 2. First, bare HMSNs were synthesized using dense silica as the core and mesoporous silica filled with CTAB as the shell, followed by selective etching of the dense silica core with Na_2CO_3. Then, HMSNs filled with CTAB surfactant in the mesopores were functionalized with sulfhydryl group by reacting with thiol-based silane coupling agent MPTS in toluene. The presence of CTAB inside the mesopores could prompt MPTS to selectively graft on the exterior surface of HMSNs rather than the internal surface of mesopore channels. Subsequently, the template CTAB inside the mesopores was removed by refluxing in methanol solution of hydrochloric acid to afford HMSNs-SH. Furthermore, HMSNs-NH_2 containing terminal amino group with disulfide bond linkage in between was obtained through the disproportionation reaction between sulfhydryl group on HMSNs-SH and pyridine group of *S*-(2-aminoethylthio)-2-thiopyridine. The morphology of HMSNs-NH_2 was characterized by SEM and TEM (Figure 1a, c, e), where the spherical HMSNs with uniform hollow structure and well-defined mesoporous shell were observed. The average diameter of the nanoparticles was about 150 nm, whereas the average thickness of the mesoporous shell was determined to be around 20 nm. The mesopores were homogeneously arranged, endowing efficient channels for the diffusion of the loaded drug. Therefore, the obtained HMSNs-NH_2 could be readily used for further functionalization as stimuli-responsive drug nanocarriers.

HOOC-NBO-*i*BuBr containing ATRP initiating group was then attached onto the surface of HMSNs-NH_2 via an amidation reaction. Herein, the successful immobilization of initiating group was confirmed by XPS, FTIR, and UV−vis spectra. As revealed by XPS spectra (Figure 2), the N 1s peak intensity of HMSNs-Br increased a bit after the amidation, indicating the existence of the newly anchored ATRP initiator. Compared with FTIR spectrum of HMSNs-NH_2 (Figure 3a), new weak peaks around 1730 and 1550 cm^{-1} in the FTIR

DOI: 10.1021/acsami.5b05893
ACS Appl. Mater. Interfaces 2015, 7, 18179−18187

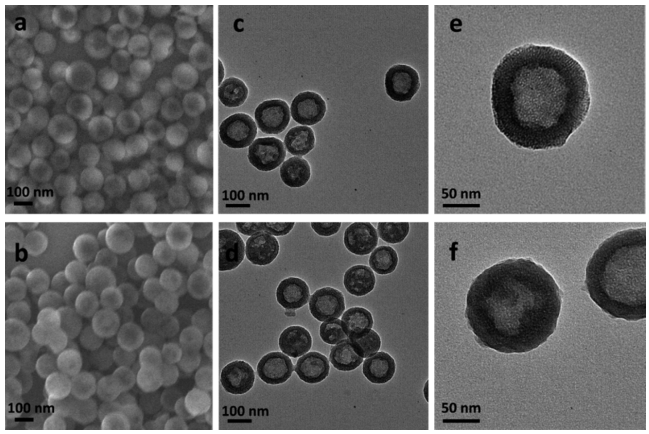

Figure 1. SEM images of (a) HMSNs-NH_2 and (b) HMSNs-PDEAEMA. TEM images of (c, e) HMSNs-NH_2 and (d, f) HMSNs-PDEAEMA.

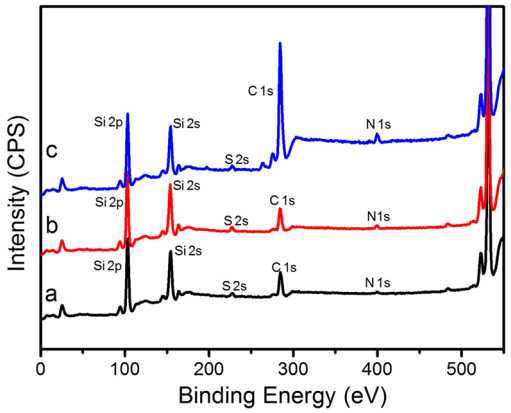

Figure 2. XPS spectra of (a) HMSNs-NH_2, (b) HMSNs-Br, and (c) HMSNs-PDEAEMA.

spectrum of HMSNs-Br (Figure 3b) were observed, ascribing to the stretching vibration of newly introduced ester carbonyl group and the N−H bending vibration of the formed secondary amine. Owing to strong background absorption of HMSNs-NH_2 (especially at low wavelength range), only a weak absorbance peak of HMSNs-Br at 302 nm was observed (Figure S4), which is consistent with characteristic absorbance peak of the HOOC-NBO-*i*BuBr linker.

The pH-sensitive polymer PDEAEMA was grafted onto the mesoporous shell via surface-initiated ATRP. TEM images of HMSNs-PDEAEMA (Figure 1d, f) clearly show that the mesopore structure became blurry in comparison with that of the original HMSNs-NH_2 (Figure 1c, e), due to the grafting of the formed polymer on the mesoporous shell. Compared with the XPS spectrum of HMSNs-Br (Figure 2b), both C 1s and N 1s peaks of HMSNs-PDEAEMA (Figure 2c) increased significantly on account of the introduction of PDMAEMA. Consistently, a strong absorption peak appeared at 1730 cm^{-1} in the FTIR spectrum of HMSNs-PDEAEMA (Figure 3c), attributing to the stretching vibration of ester carbonyl group on the grafted PDEAEMA. Furthermore, the increased adsorption peak appeared at 2953 cm^{-1} was assigned to the stretching vibration of the C−H bond on the coated polymer. All the characterizations of TEM, XPS, and FTIR discussed above confirm successful immobilization of PDEAEMA polymer on HMSNs.

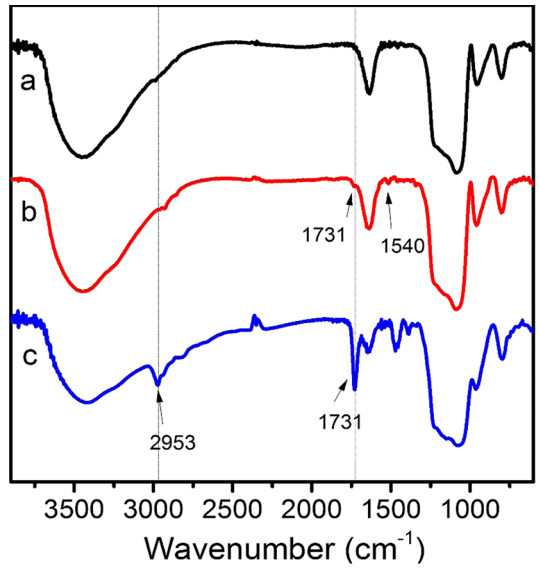

Figure 3. FTIR spectra of (a) HMSNs-NH_2, (b) HMSNs-Br, and (c) HMSNs-PDMAEMA.

The amount of grafted PDEAEMA could be roughly assessed by thermogravimetric analysis. It is well-known that the silica materials can endure high temperature while organic functionalities would be decomposed, thus leading to the weight loss of the hybrid nanoparticles upon heating. The results (Figure S5 in the Supporting Information) indicate that the weight losses of HMSNs-NH_2, HMSNs-Br, and HMSNs-PDEAEMA were 16.6, 18.3, and 35.3%, respectively, when the temperature reached 1000 °C. The difference between the weight loss of HMSNs-NH_2 and HMSNs-Br was about 1.9%, which is attributed to the modification of the initiator. By comparing the weight loss of HMSNs-Br with HMSNs-PDEAEMA, the grafting ratio of PDEAEMA was about 17.0%. To further confirm the polymer structure grafted on the surface of HMSNs, we etched the silica nanoparticles by HF solution, and the cleaved polymer was purified by dialysis against deionized water. According to ^1H NMR spectrum (Figure S6 in the Supporting Information) of the obtained polymer, all the characteristic proton signals of the PDEAEMA polymer could be found, confirming the successful grafting of PDEAEMA on the HMSNs.

The surface-initiated ATRP of DEAEMA should take place on the exterior surface of mesoporous silica shell, because HMSNs-NH_2 was functionalized with the initiating group before removing the surfactant.[22,47] Therefore, the PDEAEMA coating would not compromise the porosity of resulted HMSNs. To investigate the availability of the pore structure from the synthesized nanoparticles, we measured the nitrogen adsorption/desorption isotherms (Figure 4 and Table S1). All the isotherms of the samples exhibit characteristic type *IV* N_2 adsorption/desorption patterns, indicating the presence of mesopore channels in the nanoparticles. The specific surface area and pore volume of HMSNs-NH_2 were calculated to be 1571 $m^2\ g^{-1}$ and 1.208 mL g^{-1}, respectively, with a uniform pore size distribution of about 4.11 nm in diameter. After the modification with the initiator, the specific surface area (1495 $m^2\ g^{-1}$) and pore volume (1.189 mL g^{-1}) of HMSNs-Br decreased slightly. When the surface of the nanoparticles were coated with PDEAEMA, the specific surface area and pore volume of HMSNs-PDEAEMA decreased dramatically to 433

DOI: 10.1021/acsami.5b05893
ACS Appl. Mater. Interfaces 2015, 7, 18179−18187

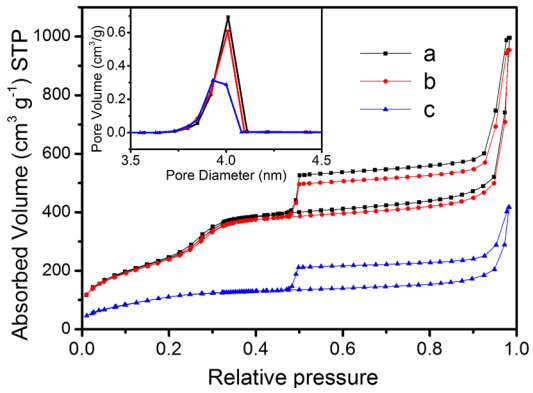

Figure 4. N_2 adsorption/desorption isotherms and (inset) corresponding pore size distributions of (a) HMSNs-NH_2, (b) HMSNs-Br, and (c) HMSNs-PDEAEMA.

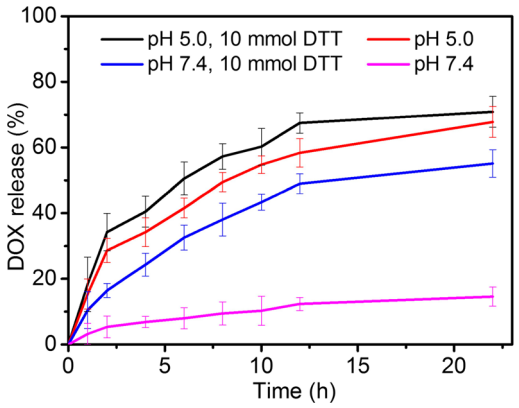

Figure 5. In vitro DOX release of HMSNs@DOX at 37 °C under different pH values without and with DTT: (a) pH 7.4, (b) pH 5.0, (c) pH 7.4 and 10 mM DTT, and (d) pH 5.0 and 10 mM DTT.

m^2 g^{-1} and 0.599 mL g^{-1}, respectively, which are consistent with the pore changes reported in literature.[24] The decrease should be attributed to the structure changes, because the mesopore channels were blocked by the PDEAEMA polymer during the drying treatment process. The pore size (3.92 nm) of HMSNs-PDEAEMA did not change significantly, indicating that the PDEAEMA polymer was not grafted onto the internal surface of mesopore channels.

pH-Dependent apparent zeta-potential value (ζ) change of HMSNs-PDEAEMA was then investigated (Figure S7). The ζ decreased continuously when the pH value of the HMSNs-PDEAEMA suspension increased. It can be explained that the acidic conditions incurred partial and eventually complete protonation of the grafted PDEAEMA, resulting in a positive charge state. While in neutral or alkaline conditions, the grafted PDEAEMA was deprotonated and became negatively charged. The critical pH for the electrostatic equilibrium of HMSNs-PDEAEMA was determined at about 7.2, which means that PDEAEMA should be deprotonated at pH value of blood circulation (pH 7.4). On the basis of this observation, PDEAEMA can be established as pH-dependent gatekeeper on the surface of HMSNs for pH-controlled drug delivery.

3.2. Loading and Triggered Release of DOX. DOX served as the model drug to be loaded into HMSNs-PDEAEMA for controlled drug delivery. At acidic conditions, because of the protonation of tertiary amine, positively charged PDEAEMA would become hydrophilic, so that it more likely stretches into water and makes the mesopores open for the DOX loading. When transferred to PBS (pH 7.4), deprotonated PDEAEMA polymer chains turn back to hydrophobic and aggregate on the surface of HMSNs to block the mesopores, thus inhibiting the release of DOX. The reversible pH-responsive behavior of PDEAEMA allows for easy DOX loading by changing the pH values of the suspension. The DOX loading efficiency was determined to be 64.5%, while the drug loading content of HMSNs-PDEAEMA reached 20.5% that is much higher than that of conventional MSNs (less than 10%). The high drug loading capacity is attributed to the hollow space serving as extra reservoirs for the drug storage.

The triggered release of DOX from HMSNs@DOX was investigated by the dialysis method in buffer medium at 37 °C under the following conditions: (i) pH 7.4, (ii) pH 5.0, (iii) pH 7.4 with 10 mM DTT, (iv) pH 5.0 with 10 mM DTT, and (v) pH 7.4 and irradiated with UV light intermittently. As shown in Figure 5, less than 12% of encapsulated DOX was released from HMSNs@DOX after the continuous incubation at pH 7.4 for 22 h, indicating good blocking capability of the grafted PDEAEMA polymer. In weak acidic environment at pH 5.0, approximately 64% of the loaded DOX was released during the same period of time. This result confirms the hypothesis that the protonation of grafted PDEAEMA could lead to the opening of the mesopores for drug release. In addition, the release of DOX at pH 7.4 could be accelerated by the addition of DTT through the reduction-induced cleavage of disulfide bond, since 52% of loaded DOX was released after 22 h. The synergistic effect under the two stimuli for the drug release was also observed. After the treatment with a medium at pH 5.0 together with 10 mM DTT, it exhibited the fattest and most complete release of loaded DOX, confirming that HMSNs@DOX could achieve triggered drug release under acid and/or reductive environment. Because the intracellular acidity and the level of reducing agents in many types of cancer cells are much higher than those in normal cells, such drug-loaded nanocarriers are capable of efficiently releasing the loaded drugs in specific intracellular environment of cancer cells.

To demonstrate the capability of light triggered DOX release, we subjected HMSNs@DOX to intermittent treatment with UV irradiation. As shown in Figure 6, in the absence of the UV irradiation, only a slight drug release was observed over time, indicating that the DOX was successfully blocked inside HMSNs-PDEAEMA. After the first round of UV irradiation begun at the fourth hour for 10 min, the cumulative release of

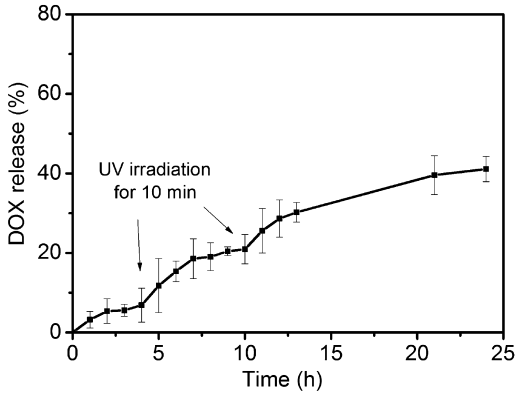

Figure 6. UV light-triggered DOX release from HMSNs@DOX at pH 7.4 with UV irradiation starting from the points indicated by arrows.

DOI: 10.1021/acsami.5b05893
ACS Appl. Mater. Interfaces 2015, 7, 18179−18187

DOX increased significantly. The same trend was again observed when the UV irradiation was repeated at the tenth hour. The triggered drug release was attributed to the rapid cleavage of the ONB linkage under UV irradiation. Thus, these results clearly indicate that HMSNs@DOX is capable of releasing the encapsulated drugs when it is triggered by any stimulus of acid environment, reducing agent, or UV irradiation.

3.3. Cellular Uptake and Intracellular Release. CLSM was applied to visualize the cellular uptake and intracellular DOX release of HMSNs@DOX in HeLa cancer cells. Meanwhile, the cells incubated with free DOX were used as the control. After incubation with free DOX for 3 h, almost all of the red fluorescence from DOX was accumulated in the nucleus regions, as observed from Figure 7. This result

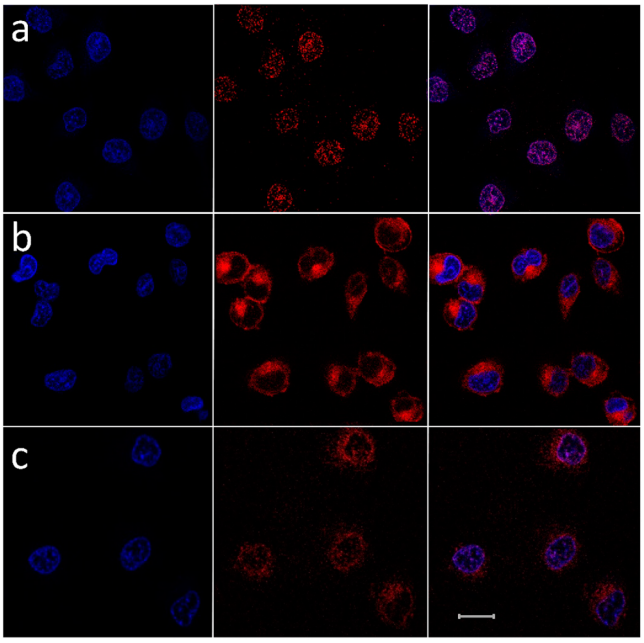

Figure 7. CLSM images of HeLa cells incubated with (a) free DOX for 3 h incubation, (b) HMSNs@DOX for 6 h incubation, and (c) HMSNs@DOX for 3 h incubation followed by 10 min UV irradiation and further incubation for another 3 h. For each panel, images from left to right show the HeLa cell nuclei stained by DAPI (blue), DOX fluorescence in cells (red), and overlay of both images. The scale bar corresponds to 20 μm.

demonstrates that free DOX could rapidly enter HeLa cells by passive diffusion and then strongly interact with DNA inside the nuclei. After 6 h incubation with HMSNs@DOX, the DOX fluorescence existed mostly in the perinucleolar regions and partly within the nuclei, indicating fast internalization of HMSNs@DOX and a partial intracellular release of encapsulated DOX. After being exposed to UV irradiation, stronger DOX fluorescence intensity was displayed in the nuclei for the same incubating time, which was attributed to the enhanced DOX release under UV irradiation.

The "turn-on" intracellular DOX release from HMSNs@DOX under UV irradiation was also confirmed by flow cytometry studies. As observed from Figure 8, HeLa cells incubated with HMSNs@DOX under UV irradiation displayed stronger intracellular DOX fluorescence intensity as compared to the cells without UV irradiation. It was documented that the fluorescence of DOX may be self-quenched when encapsulated

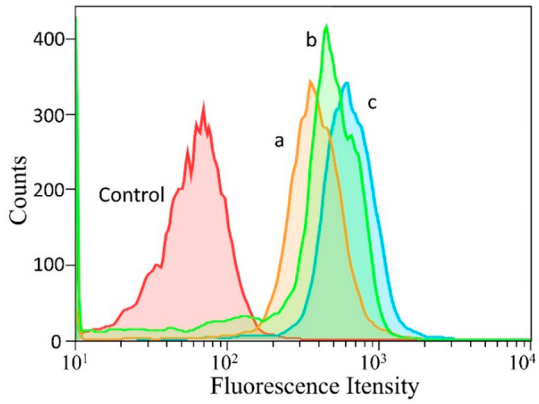

Figure 8. Flow cytometry histogram profiles of DOX florescence within HeLa cells when incubated with (a) HMSNs@DOX for 6 h incubation, (b) HMSNs@DOX for 3 h incubation followed by 10 min UV irradiation and further incubation for another 3 h, and (C) free DOX for 6 h incubation. The cells without any treatment were used as the control.

in the nanoparticles,[48,49] thus the released DOX tends to show increased fluorescence intensity when compared with its encapsulated state. Therefore, the increased DOX fluorescence intensity under UV irradiation is correlated to the "turn-on" release of DOX from the nanoparticles, which is in good agreement with the intracellular release behavior of DOX confirmed by CLSM.

3.4. Cytotoxicity Study. The in vitro cytotoxicity of HMSNs-PDEAEMA against HeLa cells was investigated by MTT assay. It was indicated in Figure 9a that HMSNs-PDEAEMA nanocarriers possessed negligible cytotoxicity, since the eventual average viability of the cells was still above 80% under a high concentration of nanocarriers applied (0.2 mg mL^{-1}). This observation verified the biocompatibility of the drug nanocarriers themselves. In addition, the cytotoxicity of HMSNs-PDEAEMA with UV irradiation was also conducted. It showed that the cytotoxicity of HMSNs-PDEAEMA under UV irradiation was almost the same as the unirradiated one. Evidently, the experiment demonstrates that the cellular growth of HeLa cells was not affected by UV light irradiation as well as light-cleaved byproducts.

Moreover, the anticancer activity of HMSNs@DOX with and without UV irradiation against HeLa cells was investigated, and free DOX was used as the control (Figure 9b). Free DOX shows the highest anticancer efficacy among all the experimental groups after 24 h incubation, which is consistent with the CLSM observation that free DOX could quickly diffuse into the nucleus and directly interact with DNA, inhibiting the cell growth in early stage of the treatment. When treated with HMSNs@DOX at low equivalent DOX concentrations below 2 μg mL^{-1}, the cell viabilities with or without UV irradiation did not show any significant difference. At higher concentrations, however, UV irradiation greatly enhanced the cytotoxicity of HMSNs@DOX against HeLa cells. Because of the limited amount of DOX released at low concentrations, the absolute difference in the concentration of released DOX between UV irradiated and unirradiated nanocarriers was almost negligible. Thus, UV irradiation did not confer any significant change to the cell viability. When the dosage of HMSNs@DOX was increased, UV irradiation could certainly lead to greater discrepancy in the concentration of

DOI: 10.1021/acsami.5b05893
ACS Appl. Mater. Interfaces 2015, 7, 18179−18187

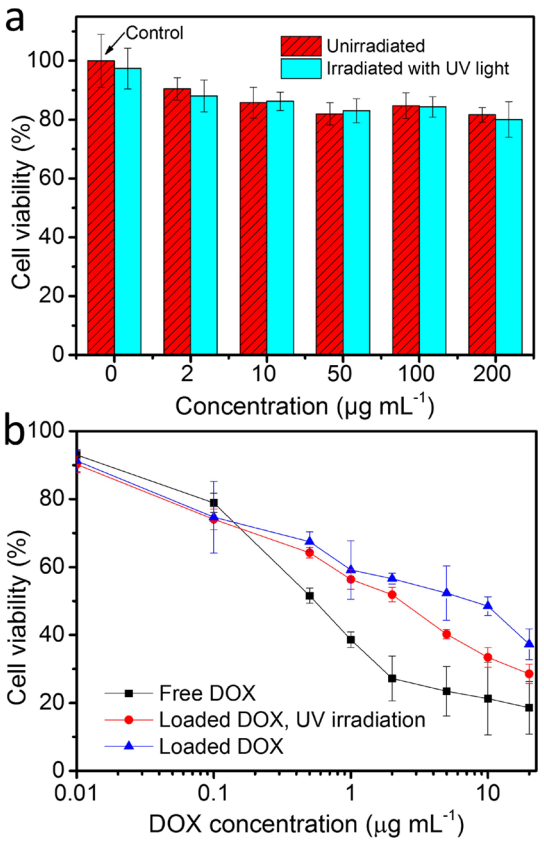

Figure 9. (a) Cytotoxicity of HMSNs-PDEAEMA nanocarriers without or with UV irradiation against HeLa cells after 24 h incubation. (b) Viability of HeLa cells treated with various doses of free DOX and HMSNs@DOX without or with UV irradiation after 24 h incubation.

active DOX between the two sample groups, widening the difference of their cell viabilities.

4. CONCLUSIONS

In summary, we have reported triple-responsive nanocarriers based on hollow mesoporous silica nanoparticles (HMSNs) coated with PDEAEMA polymer. The obtained HMSNs-PDEAEMA with multistimuli-responsive drug release capability could be used as efficient drug nanocarriers with a high loading capacity. Once entering into tumor cells, the loaded drug could be released into the cytoplasm in acid/reduction intracellular environment. Moreover, the drug release could be further enhanced by external UV irradiation. In vitro cytotoxicity assay has also confirmed that the UV irradiation could further augment the therapeutic efficacy. Compared with single stimulus responsive nanocarriers, this triple-responsive nanosystem hold greater potential for controlling the drug delivery and release process in the complicated blood circulation and pathological environment. There is no doubt that this method will enrich the drug delivery platforms based on organic–inorganic hybrids by introducing responsive polymers with special functional linkages in accordance with the practical and diverse requirements.

■ ASSOCIATED CONTENT

Ⓢ Supporting Information

The Supporting Information is available free of charge on the ACS Publications website at DOI: 10.1021/acsami.5b05893.

Additional analytical data and figures (PDF)

■ AUTHOR INFORMATION

Corresponding Author

*E-mail: zhaoyanli@ntu.edu.sg.

Author Contributions

The manuscript was written through contributions of all authors. All authors have given approval to the final version of the manuscript.

Notes

The authors declare no competing financial interest.

■ ACKNOWLEDGMENTS

This work is supported by the National Research Foundation (NRF), Prime Minister's Office, Singapore under its NRF Fellowship (NRF2009NRF-RF001-015), and Campus for Research Excellence and Technological Enterprise (CREATE) Programme–Singapore Peking University Research Centre for a Sustainable Low-Carbon Future, as well as the NTU-A*Star Silicon Technologies Centre of Excellence under the program Grant 11235100003.

■ REFERENCES

(1) Li, Z.; Barnes, J. C.; Bosoy, A.; Stoddart, J. F.; Zink, J. I. Mesoporous Silica Nanoparticles in Biomedical Applications. *Chem. Soc. Rev.* **2012**, *41*, 2590–2605.

(2) Mamaeva, V.; Sahlgren, C.; Linden, M. Mesoporous Silica Nanoparticles in Medicine-Recent Advances. *Adv. Drug Delivery Rev.* **2013**, *65*, 689–702.

(3) Tang, F.; Li, L.; Chen, D. Mesoporous Silica Nanoparticles: Synthesis, Biocompatibility and Drug Delivery. *Adv. Mater.* **2012**, *24*, 1504–1534.

(4) Wu, S. H.; Mou, C. Y.; Lin, H. P. Synthesis of Mesoporous Silica Nanoparticles. *Chem. Soc. Rev.* **2013**, *42*, 3862–3875.

(5) Jain, R. K.; Stylianopoulos, T. Delivering Nanomedicine to Solid Tumors. *Nat. Rev. Clin. Oncol.* **2010**, *7*, 653–664.

(6) Argyo, C.; Weiss, V.; Bräuchle, C.; Bein, T. Multifunctional Mesoporous Silica Nanoparticles as a Universal Platform for Drug Delivery. *Chem. Mater.* **2014**, *26*, 435–451.

(7) Hudson, S. P.; Padera, R. F.; Langer, R.; Kohane, D. S. The Biocompatibility of Mesoporous Silicates. *Biomaterials* **2008**, *29*, 4045–4055.

(8) Di Pasqua, A. J.; Sharma, K. K.; Shi, Y.-L.; Toms, B. B.; Ouellette, W.; Dabrowiak, J. C.; Asefa, T. Cytotoxicity of Mesoporous Silica Nanomaterials. *J. Inorg. Biochem.* **2008**, *102*, 1416–1423.

(9) Fang, X.; Chen, C.; Liu, Z.; Liu, P.; Zheng, N. A Cationic Surfactant Assisted Selective Etching Strategy to Hollow Mesoporous Silica Spheres. *Nanoscale* **2011**, *3*, 1632–1639.

(10) Ma, X.; Qu, Q.; Zhao, Y. Targeted Delivery of 5-Aminolevulinic Acid by Multifunctional Hollow Mesoporous Silica Nanoparticles for Photodynamic Skin Cancer Therapy. *ACS Appl. Mater. Interfaces* **2015**, *7*, 10671–10676.

(11) Slowing, II; Vivero-Escoto, J. L.; Wu, C. W.; Lin, V. S. Mesoporous Silica Nanoparticles as Controlled Release Drug Delivery and Gene Transfection Carriers. *Adv. Drug Delivery Rev.* **2008**, *60*, 1278–1288.

(12) Zhang, Y.; Hsu, B. Y.; Ren, C.; Li, X.; Wang, J. Silica-Based Nanocapsules: Synthesis, Structure Control and Biomedical Applications. *Chem. Soc. Rev.* **2015**, *44*, 315–335.

(13) Yang, P.; Gai, S.; Lin, J. Functionalized Mesoporous Silica Materials for Controlled Drug Delivery. *Chem. Soc. Rev.* **2012**, *41*, 3679–3698.

(14) Lai, C.-Y.; Trewyn, B. G.; Jeftinija, D. M.; Jeftinija, K.; Xu, S.; Jeftinija, S.; Lin, V. S. Y. A Mesoporous Silica Nanosphere-Based Carrier System with Chemically Removable CdS Nanoparticle Caps

DOI: 10.1021/acsami.5b05893
ACS Appl. Mater. Interfaces 2015, 7, 18179–18187

for Stimuli-Responsive Controlled Release of Neurotransmitters and Drug Molecules. *J. Am. Chem. Soc.* **2003**, *125*, 4451−4459.
(15) Wang, Y.; Wang, K.; Zhao, J.; Liu, X.; Bu, J.; Yan, X.; Huang, R. Multifunctional Mesoporous Silica-Coated Graphene Nanosheet Used for Chemo-Photothermal Synergistic Targeted Therapy of Glioma. *J. Am. Chem. Soc.* **2013**, *135*, 4799−4804.
(16) Li, M.; Yan, H.; Teh, C.; Korzh, V.; Zhao, Y. NIR-Triggered Drug Release from Switchable Rotaxane-Functionalized Silica-Covered Au Nanorods. *Chem. Commun.* **2014**, *50*, 9745−9748.
(17) Guardado-Alvarez, T. M.; Sudha Devi, L.; Russell, M. M.; Schwartz, B. J.; Zink, J. I. Activation of Snap-Top Capped Mesoporous Silica Nanocontainers Using Two Near-Infrared Photons. *J. Am. Chem. Soc.* **2013**, *135*, 14000−14003.
(18) Zhang, Z.; Balogh, D.; Wang, F.; Sung, S. Y.; Nechushtai, R.; Willner, I. Biocatalytic Release of an Anticancer Drug from Nucleic-Acids-Capped Mesoporous SiO_2 Using DNA or Molecular Biomarkers as Triggering Stimuli. *ACS Nano* **2013**, *7*, 8455−8468.
(19) Lee, J.; Kim, H.; Han, S.; Hong, E.; Lee, K. H.; Kim, C. Stimuli-Responsive Conformational Conversion of Peptide Gatekeepers for Controlled Release of Guests from Mesoporous Silica Nanocontainers. *J. Am. Chem. Soc.* **2014**, *136*, 12880−12883.
(20) Zhang, Y.; Wang, Z.; Zhou, W.; Min, G.; Lang, M. Cationic Poly(ε-Caprolactone) Surface Functionalized Mesoporous Silica Nanoparticles and Their Application in Drug Delivery. *Appl. Surf. Sci.* **2013**, *276*, 769−775.
(21) Lee, E. S.; Gao, Z.; Bae, Y. H. Recent Progress in Tumor pH Targeting Nanotechnology. *J. Controlled Release* **2008**, *132*, 164−170.
(22) Sun, J.-T.; Hong, C.-Y.; Pan, C.-Y. Fabrication of PDEAEMA-Coated Mesoporous Silica Nanoparticles and pH-Responsive Controlled Release. *J. Phys. Chem. C* **2010**, *114*, 12481−12486.
(23) Huang, X.; Hauptmann, N.; Appelhans, D.; Formanek, P.; Frank, S.; Kaskel, S.; Temme, A.; Voit, B. Synthesis of Hetero-Polymer Functionalized Nanocarriers by Combining Surface-Initiated ATRP and RAFT Polymerization. *Small* **2012**, *8*, 3579−3583.
(24) Mei, X.; Chen, D.; Li, N.; Xu, Q.; Ge, J.; Li, H.; Lu, J. Hollow Mesoporous Silica Nanoparticles Conjugated with pH-Sensitive Amphiphilic Diblock Polymer for Controlled Drug Release. *Microporous Mesoporous Mater.* **2012**, *152*, 16−24.
(25) Yuan, L.; Tang, Q.; Yang, D.; Zhang, J. Z.; Zhang, F.; Hu, J. Preparation of pH-Responsive Mesoporous Silica Nanoparticles and Their Application in Controlled Drug Delivery. *J. Phys. Chem. C* **2011**, *115*, 9926−9932.
(26) Liu, R.; Zhao, X.; Wu, T.; Feng, P. Tunable Redox-Responsive Hybrid Nanogated Ensembles. *J. Am. Chem. Soc.* **2008**, *130*, 14418−14419.
(27) Ji, W.; Li, N.; Chen, D.; Qi, X.; Sha, W.; Jiao, Y.; Xu, Q.; Lu, J. Coumarin-Containing Photo-Responsive Nanocomposites for NIR Light-Triggered Controlled Drug Release *via* a Two-Photon Process. *J. Mater. Chem. B* **2013**, *1*, 5942−5949.
(28) Lai, J.; Mu, X.; Xu, Y.; Wu, X.; Wu, C.; Li, C.; Chen, J.; Zhao, Y. Light-Responsive Nanogated Ensemble Based on Polymer Grafted Mesoporous Silica Hybrid Nanoparticles. *Chem. Commun.* **2010**, *46*, 7370−7372.
(29) Xing, Q.; Li, N.; Chen, D.; Sha, W.; Jiao, Y.; Qi, X.; Xu, Q.; Lu, J. Light-Responsive Amphiphilic Copolymer Coated Nanoparticles as Nanocarriers and Real-Time Monitors for Controlled Drug Release. *J. Mater. Chem. B* **2014**, *2*, 1182−1189.
(30) Mei, X.; Yang, S.; Chen, D.; Li, N.; Li, H.; Xu, Q.; Ge, J.; Lu, J. Light-Triggered Reversible Assemblies of Azobenzene-Containing Amphiphilic Copolymer with Beta-Cyclodextrin-Modified Hollow Mesoporous Silica Nanoparticles for Controlled Drug Release. *Chem. Commun.* **2012**, *48*, 10010−10012.
(31) Cao, Z.; Wu, H.; Dong, J.; Wang, G. Quadruple-Stimuli-Sensitive Polymeric Nanocarriers for Controlled Release under Combined Stimulation. *Macromolecules* **2014**, *47*, 8777−8783.
(32) Wu, H.; Dong, J.; Li, C.; Liu, Y.; Feng, N.; Xu, L.; Zhan, X.; Yang, H.; Wang, G. Multi-Responsive Nitrobenzene-Based Amphiphilic Random Copolymer Assemblies. *Chem. Commun.* **2013**, *49*, 3516−3518.
(33) Cheng, R.; Meng, F.; Deng, C.; Klok, H. A.; Zhong, Z. Dual and Multi-Stimuli Responsive Polymeric Nanoparticles for Programmed Site-Specific Drug Delivery. *Biomaterials* **2013**, *34*, 3647−3657.
(34) Schattling, P.; Jochum, F. D.; Theato, P. Multi-Stimuli Responsive Polymers − The All-in-One Talents. *Polym. Chem.* **2014**, *5*, 25−36.
(35) Xiao, D.; Jia, H. Z.; Zhang, J.; Liu, C. W.; Zhuo, R. X.; Zhang, X. Z. A Dual-Responsive Mesoporous Silica Nanoparticle for Tumor-Triggered Targeting Drug Delivery. *Small* **2014**, *10*, 591−598.
(36) Liu, X.; Yu, D.; Jin, C.; Song, X.; Cheng, J.; Zhao, X.; Qi, X.; Zhang, G. A Dual Responsive Targeted Drug Delivery System Based on Smart Polymer Coated Mesoporous Silica for Laryngeal Carcinoma Treatment. *New J. Chem.* **2014**, *38*, 4830−4836.
(37) Lee, A. S.; Gast, A. P.; Bütün, V.; Armes, S. P. Characterizing the Structure of pH Dependent Polyelectrolyte Block Copolymer Micelles. *Macromolecules* **1999**, *32*, 4302−4310.
(38) Lobb, E. J.; Ma, I.; Billingham, N. C.; Armes, S. P.; Lewis, A. L. Facile Synthesis of Well-Defined, Biocompatible Phosphorylcholine-Based Methacrylate Copolymers *via* Atom Transfer Radical Polymerization at 20 °C. *J. Am. Chem. Soc.* **2001**, *123*, 7913−7914.
(39) Zhang, Y.; Qu, Q.; Li, M.; Zhao, Y. Intracellular Reduction-Responsive Sheddable Copolymer Micelles for Targeted Anticancer Drug Delivery. *Asian J. Org. Chem.* **2015**, *4*, 226−232.
(40) Meng, F.; Hennink, W. E.; Zhong, Z. Reduction-Sensitive Polymers and Bioconjugates for Biomedical Applications. *Biomaterials* **2009**, *30*, 2180−2198.
(41) Gohy, J. F.; Zhao, Y. Photo-Responsive Block Copolymer Micelles: Design and Behavior. *Chem. Soc. Rev.* **2013**, *42*, 7117−7129.
(42) Liu, G.; Liu, W.; Dong, C.-M. UV- and NIR-Responsive Polymeric Nanomedicines for On-Demand Drug Delivery. *Polym. Chem.* **2013**, *4*, 3431−3443.
(43) Li, Y.; Xiao, K.; Zhu, W.; Deng, W.; Lam, K. S. Stimuli-Responsive Cross-Linked Micelles for On-Demand Drug Delivery against Cancers. *Adv. Drug Delivery Rev.* **2014**, *66*, 58−73.
(44) Tyrrell, Z. L.; Shen, Y.; Radosz, M. Fabrication of Micellar Nanoparticles for Drug Delivery through the Self-Assembly of Block Copolymers. *Prog. Polym. Sci.* **2010**, *35*, 1128−1143.
(45) Schumers, J.-M.; Gohy, J.-F.; Fustin, C.-A. A Versatile Strategy for the Synthesis of Block Copolymers Bearing a Photocleavable Junction. *Polym. Chem.* **2010**, *1*, 161−163.
(46) Luo, Z.; Ding, X.; Hu, Y.; Wu, S.; Xiang, Y.; Zeng, Y.; Zhang, B.; Yan, H.; Zhang, H.; Zhu, L.; Liu, J.; Li, J.; Cai, K.; Zhao, Y. Engineering a Hollow Nanocontainer Platform with Multifunctional Molecular Machines for Tumor-Targeted Therapy *in Vitro* and *in Vivo*. *ACS Nano* **2013**, *7*, 10271−10284.
(47) Chung, P.-W.; Kumar, R.; Pruski, M.; Lin, V. S. Y. Temperature Responsive Solution Partition of Organic−Inorganic Hybrid Poly(*N*-Isopropylacrylamide)-Coated Mesoporous Silica Nanospheres. *Adv. Funct. Mater.* **2008**, *18*, 1390−1398.
(48) Ding, J.; Shi, F.; Xiao, C.; Lin, L.; Chen, L.; He, C.; Zhuang, X.; Chen, X. One-Step Preparation of Reduction-Responsive Poly(Ethylene Glycol)-Poly(Amino Acid)s Nanogels as Efficient Intracellular Drug Delivery Platforms. *Polym. Chem.* **2011**, *2*, 2857−2864.
(49) Matsumura, Y.; Kataoka, K. Preclinical and Clinical Studies of Anticancer Agent-Incorporating Polymer Micelles. *Cancer Sci.* **2009**, *100*, 572−579.

DOI: 10.1021/acsami.5b05893
ACS Appl. Mater. Interfaces 2015, 7, 18179−18187